Journal of Inflammation Research

Dovepress
Taylor & Francis Group

Open Access Full Text Article

ORIGINAL RESEARCH

New Bitongling Ameliorates Joint Tissue Damage in Collagen-Induced Arthritis Mice by Suppressing Mapt Expression: A Genome-Wide Sequencing Study

Yunke Guo[1,*], Mengjiang Tian[2,*], Yang Liu[2], Jue Ma[2], Yang Li[2], Yu Hou[3], Yue Wang[1]

[1]Department of Rheumatism, Affiliated Hospital of Nanjing University of Chinese Medicine, Nanjing, Jiangsu, 210029, People's Republic of China; [2]Department of Rheumatism, Traditional Chinese Medicine Hospital of Ili Kazakh Autonomous Prefecture, Ili, Xinjiang, 835000, People's Republic of China; [3]First Clinical Medical College, Nanjing University of Chinese Medicine, Nanjing, Jiangsu, 210029, People's Republic of China

*These authors contributed equally to this work

Correspondence: Yue Wang, Department of Rheumatism, Affiliated Hospital of Nanjing University of Chinese Medicine, No. 155 Hanzhong Road, Qinhuai District, Nanjing, Jiangsu, 210029, People's Republic of China, Email wangyue2020l@163.com

Objective: Rheumatoid arthritis (RA) affects 1% of the global population, with joint destruction leading to disability. While current biologics (eg, TNF-α inhibitors) and small-molecule therapies (eg, JAK inhibitors) have significantly improved symptom control and slowed radiographic progression in many patients, unresolved challenges remain in simultaneously addressing mitochondrial dysfunction and synovial inflammation—the core drivers of joint destruction. This study aimed to investigate the molecular mechanism by which New Bitongling (NBTL) mitigates joint damage in collagen-induced arthritis (CIA) mice through regulation of the microtubule-associated protein tau (Mapt).

Methods: Male C57BL/6 mice (6 weeks old, specific pathogen-free) were used to establish the collagen-induced arthritis (CIA) model and randomly assigned to three groups: control, model, and NBTL intervention. Clinical symptoms were evaluated using the arthritis index (AI), paw swelling volume (measured by water displacement), and behavioral tests (sucrose preference test and open-field test). Histopathological changes were assessed via hematoxylin-eosin (HE) and Safranin O-Fast Green staining. Molecular mechanisms were analyzed using Western blotting, flow cytometry, and mitochondrial membrane potential (JC-1 staining) assays. Western blotting analyzed apoptosis-related proteins and the Sirtuin 1 (Sirt1)/Peroxisome proliferator-activated receptor γ coactivator 1α (PGC-1α) pathway, flow cytometry measured reactive oxygen species (ROS) levels, and JC-1 fluorescence staining evaluated mitochondrial membrane potential. Genome-wide sequencing identified Mapt as the key target, with functional validation conducted through siRNA knockdown and adeno-associated virus (AAV) Mapt overexpression. Statistical analyses included repeated-measures Analysis of Variance (ANOVA) with Tukey's post-hoc test and $P<0.05$ was considered significant.

Results: NBTL treatment significantly reduced AI scores, paw swelling, and joint deformities while improving behavioral indicators. Histological analysis revealed attenuated synovial inflammation, pannus formation, and bone erosion in the NBTL group. Moreover, pro-inflammatory mediators were downregulated in NBTL-treated mice, accompanied by reduced Bax/cleaved-caspase3 and elevated Bcl-2 expression ($P<0.05$). NBTL restored mitochondrial membrane potential, activated the Sirt1/PGC-1α pathway, reduced ROS levels, and decreased oxidative stress damage ($P<0.05$). Mapt overexpression exacerbated joint damage, whereas Mapt silencing or NBTL intervention reversed these effects. Genome-wide sequencing confirmed that NBTL modulates mitochondrial homeostasis and inflammatory responses via Mapt inhibition.

Conclusion: This study demonstrates that New bitongling ameliorates joint damage in collagen-induced arthritis mice by suppressing microtubule-associated protein tau expression, restoring mitochondrial function, and modulating synovial inflammation. These findings provide preclinical evidence supporting further investigation of New bitongling as a novel therapeutic agent for rheumatoid arthritis.

Keywords: new bitongling, rheumatoid arthritis, Mapt protein, gastrointestinal microbiome, Sirtuin 1

Received: 31 July 2025
Accepted: 29 October 2025
Published: 8 November 2025

Introduction

With its increasing global prevalence, rheumatoid arthritis (RA; ICD-10: M05-M06) has become a major public health concern due to its irreversible joint damage, significant impairment of patients' quality of life, and substantial socio-economic burden.[1,2] Conventional treatments for RA, including nonsteroidal anti-inflammatory drugs (NSAIDs), disease-modifying antirheumatic drugs (DMARDs), and biologics (eg, TNF-α inhibitors), have demonstrated considerable efficacy in managing symptoms, reducing systemic inflammation, and slowing radiographic progression in a majority of patients. However, their ability to simultaneously address mitochondrial dysfunction and synovial inflammation—two synergistic drivers of joint destruction—remains limited. For instance, while TNF-α inhibitors effectively suppress pro-inflammatory cytokines, they do not directly restore mitochondrial homeostasis or inhibit chondrocyte pyroptosis.[3] Recent advances in Janus kinase (JAK) inhibitors (eg, tofacitinib) show promise in modulating immune pathways and improving clinical outcomes, yet concerns regarding long-term safety profiles and sustained efficacy persist.[4] These gaps underscore the urgent need for novel therapies that integrate anti-inflammatory, mitochondria-protective, and chondro-protective mechanisms. Traditional Chinese medicine (TCM) formulations, such as New Bitongling (NBTL), offer a multi-target synergistic approach,[5] with emerging evidence suggesting potential benefits in RA treatment.[6,7] Recently, Guan et al put forward the view that NBTL can improve the progress of RA by regulating intestinal flora.[8] However, these theories have not been confirmed by definite studies. At present, we do not know the specific mechanism of NBTL in RA, which also makes it difficult to promote the use of NBTL in the world. Meanwhile, its clinical translation is limited by variable herb composition, undefined active ingredients, and lack of standardized dosing regimens. Further clinical trials are needed to validate its safety and efficacy in humans.

This study combined whole-genome sequencing (WGS) technology with the collagen-induced arthritis (CIA) mouse model, systematically elucidating the multi-dimensional regulatory mechanisms through which NBTL mitigates joint damage. By constructing a spatiotemporal dynamic gene expression profile of CIA mice, we identified Mapt as the core target of NBTL. Recent reviews emphasize the urgent need for mechanistic studies on TCM formulas targeting mitochondrial dysfunction in RA.[9] Specifically, the role of Mapt in synovial tissue remains undefined,[7] despite its established role in neurodegenerative diseases. Further mechanistic investigation revealed that NBTL downregulates Mapt expression, restores mitochondrial function, and inhibits the molecular cascade driving chondrocyte pyroptosis. Unlike conventional single-pathway studies, our WGS approach transcends the limitations of known inflammatory or immune pathways, offering a comprehensive perspective on the novel mechanism by which TCM compounds regulate mitochondrial homeostasis. These findings provide original target-level evidence for RA treatment. Notably, the research has for the first time identified Mapt as a crucial regulator in RA joint damage, opening new avenues for both diagnostic and therapeutic development. Furthermore, the study elucidates the multi-dimensional pharmacological network of NBTL at the genomic level, marking an important step in transforming TCM compounds from empirical remedies to precisely targeted therapies. Most importantly, the proposed intervention strategy based on mitochondrial homeostasis reconstruction establishes a theoretical framework for developing RA treatments with reduced toxicity and prolonged efficacy, underscoring its substantial translational medical value.

Here, we integrated genome-wide sequencing with the CIA mouse model to elucidate how NBTL modulates microtubule-associated protein tau (Mapt) expression, mitochondrial function, and synovial inflammation, providing preclinical evidence for its role as a precision therapy for RA.

Materials and Methods

Animal Data

Seventy healthy, specific pathogen-free, 6-week-old male C57BL/6 mice were utilized in this study. Prior to the experiment, the animals underwent a 1-week acclimatization period. Throughout the study, wood chip bedding in the cages was replaced every other day. The animal facility maintained controlled environmental conditions, including a temperature range of 20–25°C and a 12-hour light/dark cycle. All the experimental procedures involving animals were conducted in accordance with ARRIVE guidelines, the 3R principles (Reduction, Replacement, Refinement) and approved by the Animal Ethics Committee of The Affiliated Hospital of Nanjing University of Chinese Medicine (Approval number:2025DW-035-01).

Preparation of NBTL

NBTL is a herbal formulation composed of six medicinal herbs: Ephedra (Mahuang), Cinnamon Twig (Guizhi), Saposhnikovia Root (Fangfeng), Caulis Sinomenii (Qingfengteng), Radix Aconiti Preparata (Zhi Chuanwu), and Honeycomb (Fengfang). The raw herbal materials were supplied by the pharmacy of Jiangsu Provincial Hospital of Traditional Chinese Medicine. The extraction protocol was developed by the Chinese Medicine Processing Teaching and Research Office at Nanjing University of Chinese Medicine and subsequently prepared by the pharmaceutical department of Jiangsu Provincial Hospital of Traditional Chinese Medicine. The extraction process involved the following steps: (1) Volatile oil extraction from Cinnamon Twig and other relevant herbs; (2) Ethanol extraction of Ephedra and other specified herbs, and; (3) Aqueous extraction of Radix Aconiti Preparata and additional herbs. The ethanol was then recovered under reduced pressure until the extract was completely alcohol-free. The final NBTL extract was concentrated to a density of 2.299 g/mL.

Grouping and Intervention

Following one week of adaptive feeding, 30 mice were randomly allocated into three groups (10 rats in each group per group). The control group received standard feeding, while the other two groups were subjected to CIA modeling.[10] For CIA induction, immunogenic chicken type II collagen was thawed at 4°C for 20 minutes, and complete Freund's adjuvant (CFA) was pre-cooled on crushed ice. Next, the CFA was injected into a glass test tube. While stirring with a homogenizer, an equal volume of chicken type II collagen was slowly added, followed by thorough emulsification for 20–25 minutes. The emulsion was considered adequately prepared when a droplet did not disperse upon contact with water. The final concentration of the chicken type II collagen–CFA emulsion was adjusted to 1 mg/mL. For primary immunization, 0.1 mL of the emulsion was administered via subcutaneous injection at the left base of the tail in each mouse. A booster immunization was performed 21 days later by injecting 0.1 mL at the right base of the tail. Post-injection, the Arthritis Index (AI)[11] was evaluated every four days, with an AI score = 4 indicating successful CIA induction. Upon successful modeling, the CIA mice were further randomized into two groups. One group received NBTL via oral gavage at a daily dose of 1.6 g/kg (the dose used is based on the body weight of human and mouse) for 21 consecutive days (designated as the NBTL group), while the other group was administered an equivalent volume of distilled water (designated as the model group).

Clinical Symptom Assessment

Following the completion of the above intervention procedures, the left hind paw volume of mice was measured using the water displacement method with a paw swelling meter. Subsequently, the AI score was evaluated. AI scoring, a validated semiquantitative measure of joint inflammation,[12] was performed by two blinded observers. Paw swelling was measured using a digital caliper (Mitutoyo, Japan) with intra-class correlation coefficient (ICC) >0.9. Score 0: no swelling or erythema; Score 1: slight erythema or swelling limited to the feet; Score 2: obvious erythema or swelling involving all feet; Score 3: erythema or swelling spreading to adjacent tissues; Score 4: severe swelling with elevated skin temperature and limited activity.

Behavioral Tests

Sucrose preference test: On day 1, two bottles containing an equal volume of 1% sucrose solution were placed in each cage. On day 2, one bottle of pure water and one bottle of 1% sucrose solution (equal volume) were randomly positioned, with their locations switched after 12 hours. On day 3, mice were subjected to 24-hour food and water deprivation. The formal experiment then commenced: each rat was provided with equal volumes of pure water and 1% sucrose solution. After 1 hour, the remaining volumes of both liquids were measured and the sucrose preference rate (%) was calculated.

Open-field test: In a quiet environment, mice were gently held by the base of their tails and placed in the center of an open-field test case. After a 30-second acclimatization period, horizontal activity (total number of squares crossed) and vertical activity (number of rearing events) were recorded over 5 minutes using an animal movement tracking system (Noldus, EthoVision XT).

Behavioral tests (sucrose preference and open-field tests) were conducted in a soundproof room following the Standardized Health and Research Phenotyping Assay (SHIRPA) protocol.

Hematoxylin - Eosin (HE) Staining of Joint Tissue

Following the completion of the aforementioned tests, the mice were euthanized via anesthetic overdose. The ankle joint tissue was harvested, fixed for 24 hours, and subsequently subjected to decalcification, dehydration, and transparency treatments. The samples were then paraffin-embedded and sectioned into 4 μm slices. After dewaxing and rehydration, HE staining was performed. Finally, the stained sections were mounted and examined under an optical microscope to evaluate pathological changes in the synovial tissue.

Enzyme-Linked Immunosorbent Assay (ELISA)

Approximately 3–5 mL of blood was collected from the abdominal aorta and centrifuged to isolate serum. The serum levels of Matrix metalloproteinase-3 (MMP-3), Tumor necrosis factor-α (TNF-α), Interleukin-1β (IL-1β), and Interleukin-10 (IL-10) were quantified using ELISA.

Colorimetric Method

Mouse joint tissues were lysed by RIPA for 30 min, ground, washed three times with PBS, 10% tissue homogenate was prepared, centrifuged at12000r-min-1 for 15 min (centrifugation radius 13 cm), and the supernatant was extracted for total protein. Total protein was extracted from the supernatant. The levels of Malondialdehyde (MDA), Superoxide dismutase (SOD) and Glutathione (GSH) were measured by colorimetric method.

Flow Cytometry Analysis

The joint tissue was minced and enzymatically digested with collagenase IV. Subsequently, DCFH-DA was added and incubated in the dark for 30 minutes. Total reactive oxygen species (ROS) levels were assessed by measuring 2′,7′-dichlorofluorescein (DCF) fluorescence using a flow cytometer (Ex 488 nm/Em 530 nm).

Safranin O-Fast Green Staining of Synovial Tissue

Using forceps and scissors, the rat knee joint cavity was carefully opened to expose the synovial tissue, which appeared as a smooth, glossy, pale-yellow layer. The synovial tissue was gently dissected and stored at −80°C. Synovial tissue sections were prepared following the same protocol as HE staining. After baking, paraffin was removed by xylene treatment, and the sections were sequentially stained with Safranin O and Fast Green solutions. The slides were rapidly dried and mounted. Cartilage morphology was then examined and imaged under an optical microscope.

Multiplexed Protein Analysis

Tissue samples (100 mg synovium/CIA joints) underwent standardized processing: homogenization in RIPA buffer followed by bicinchoninic acid (BCA) quantification. For Western blot, 150 μg protein underwent denaturation, sodium dodecyl sulfate polyacrylamide gel electrophoresis (SDS-PAGE) separation, and nitrocellulose transfer. Membranes were blocked (5% skim milk, 2 hr RT) prior to sequential incubation with primary antibodies targeting apoptosis (Fas/FasL/Bax/cleaved caspase-3) and anti-apoptotic (Bcl-2) markers, plus β-tubulin as loading control (all 1:1000, 4°C overnight). Signal detection employed HRP-conjugated secondary antibodies (1:2000, RT, dark) with chemiluminescent imaging and densitometric quantification.

Immunohistochemistry

The paraffin sections underwent deparaffinization (xylene/graded ethanol), antigen retrieval (citrate buffer, pressure-cooking), and blocking. Primary antibodies against extracellular matrix/remodeling factors (Collagen II, MMP-3) and inflammatory cytokines [IL-6, recombinant chemokine (C-X-C motif) ligand 2/10 (CXCL2/CXCL10)] (1:200, 4°C overnight) were visualized via DAB chromogenic detection. Hematoxylin counterstaining and dehydration were standardized before ImagePro Plus-based morphometric analysis.

Mitochondrial Fluorescence Profiling

Cryo-sectioned synovial tissue (5 μm, OCT-embedded) was fixed (4% phosphofructaldolase) and permeabilized (0.1% Triton X-100). Dual staining with JC-1 (5 μg/mL, 37°C/20 min) and 4,6-diamino-2-phenyl indole (DAPI) (1 μg/mL, 5 min) enabled mitochondrial membrane potential assessment. Fluorescence intensity ratios (Ex540/Em590 vs Ex490/Em530) were quantified from confocal images using Zen software, with red/green fluorescence ratios reflecting ΔΨm status.

16S rRNA Gene Sequencing

Fresh fecal samples of an appropriate amount were collected from both the model group (labeled M) and the NBTL group (labeled X) of mice. Genomic DNA was extracted using commercial reagents. Following the selection of target regions, library preparation was performed using the NEB Next Ultra^{TM} DNA Library Prep Kit. The resulting libraries were sequenced on the MiSeq high-throughput next-generation sequencing platform, targeting the V3-V4 hypervariable regions for amplification and sequencing. Linear discriminant analysis (LDA) effect size (LEfSe) was applied for further analysis. For alpha diversity assessment (including Shannon, Simpson, and Chao1 indices), QIIME 1 (v1.8.0) was employed. Species composition bar plots were generated using R software (v3.6.0) based on taxonomic annotation and relative abundance data. Additionally, principal coordinate analysis (PCoA) was conducted based on Weighted UniFrac distances, implemented in R. Differential abundance analysis was performed using Metastats in Mothur (v1.34.4), while LEfSe analysis was carried out with Python (v2.7), applying an LDA score threshold of ≥ 3 to identify significant differences in gut microbiota relative abundance across taxonomic levels between groups. The operational taxonomic unit (OTU) abundance tables from sequencing were normalized using the PICRUSt2 (v2. 3. 0-b) software.

Target Gene Analysis of NBTL

Total RNA was extracted from tissue samples and validated for quality using Nanodrop2000 (concentration, purity), agarose gel electrophoresis (integrity), and Agilent2100 (RIN value). Library construction required ≥1μg total RNA with OD260/280 ≥1.8 and OD260/230 ≥1.0 (≥35ng/μL concentration). PolyA mRNA was isolated via Oligo(dT) magnetic beads, followed by fragmentation into ~300bp fragments using a fragmentation buffer. Double-stranded cDNA was synthesized through reverse transcription with random hexamers, second-strand synthesis, and end repair (including A-tailing for Y-adapter ligation). Indexed PE libraries (2×150bp read length) were sequenced on a second-generation platform, with differential expression defined as $|LogFC|>1$ and $P<0.05$.

Functional Enrichment Analysis of Differentially Expressed Genes (DEGs)

GO, KEGG, and KOG enrichment analyses were performed with the help of DAVID database comprehensive analysis tool (http://david.ncifcrf.gov) to screen the significantly different data ($P<0.05$), and explored the functions and pathways potentially affected by the differential genes.

Analysis of the Impact of Mapt on CIA

Forty mice were selected and subjected to CIA modeling, then divided into four groups (10 rats in each group): (1) Blank group: The mice received no treatment and were maintained under standard feeding conditions. (2) Downregulation group (gene knockdown): Mice were administered an intra-articular injection of small interfering RNA (siRNA) targeting Mapt to specifically suppress its expression. (3) Upregulation group (gene overexpression): A Mapt-overexpressing adeno-associated virus (AAV) was constructed and delivered via intra-articular injection (1×10^9 vg per joint). Synovial-specific expression was achieved using a tissue-specific promoter (eg, COL2A1). (4) NBTL + Upregulation group: In addition to the same treatment as the Upregulation group, mice received NBTL via oral gavage. To confirm the interventional efficiency, Mapt protein expression levels were assessed by Western blot using a Mapt primary antibody at a 1:1000 dilution. The experiment was subsequently repeated to evaluate the pathological changes in CIA mice following Mapt expression modulation.

Statistical Analysis

All statistical analyses were performed using SPSS 25.0 software. The normality of the data distribution was confirmed using the Shapiro–Wilk test. Results are expressed as ($\bar{x} \pm s$). Parametric data (eg, AI scores, cytokine levels) were analyzed by one-way Analysis of Variance (ANOVA) with Tukey's post-hoc test. A P-value < 0.05 was considered statistically significant.

Results

Effect of NBTL on Clinical Symptoms in CIA Mice

In the control group, no signs of redness or swelling were observed in the paws or joints of the mice, and the AI score remained at 0. In contrast, the model group displayed significant clinical manifestations following secondary immunization, with markedly elevated AI scores and severe paw swelling compared to the control group (P<0.01). Administration of NBTL in the NBTL group led to noticeable improvements in joint inflammation and deformity in CIA mice relative to the model group (P<0.05; Figure 1A). Behavioral assessments revealed that the sucrose preference rate was significantly lower in both the model and NBTL groups compared to the control group (P<0.05). However, the NBTL group demonstrated a higher preference rate than the model group (P<0.05). In the open-field test, while the total number of squares crossed and rearing events in the NBTL group remained lower than in the control group, these measures were significantly improved compared to the model group (P<0.05, Figure 1B). Histopathological analysis of joint tissues demonstrated distinct morphological differences among the groups. The control group maintained normal joint architecture, characterized by well-organized bone and cartilage tissues with regular cellular arrangement. The synovial membrane presented a smooth surface without hyperplastic changes, exhibiting only minimal inflammatory cell infiltration, while the bony structures remained intact with clearly defined margins. In stark contrast, the model group exhibited severe pathological alterations, including pronounced epithelial hyperplasia, cellular edema, and morphological distortion, along with extensive infiltration of lymphocytes, histiocytes, and multinucleated giant cells within tissues. Additionally, prominent pannus formation and substantial bone destruction were observed. Notably, the NBTL group showed significant improvement compared to the model group, with markedly reduced inflammatory cell infiltration, diminished pannus formation, and attenuated bone destruction, and overall alleviation of joint tissue damage (Figure 1C). The inflammatory factor analysis revealed that serum levels of pro-inflammatory cytokines (MMP-3, TNF-α, and IL-1β) were significantly elevated in both the model and NBTL groups compared to the control group (P<0.05), with the levels being even lower in the NBTL group compared to the model group (P<0.05). Conversely, the anti-inflammatory cytokine IL-10 was decreased in both the model and NBTL groups compared to controls, though its levels remained higher in the NBTL group than in the model group (P<0.05; Figure 1D). In the assessment of oxidative stress, MDA and ROS levels were significantly higher in the model and NBTL groups than in the control group, while antioxidant markers (SOD, and GSH-Px) were lower (P<0.05). Notably, the NBTL group exhibited significantly reduced MDA and ROS levels compared to the model group, along with elevated SOD and GSH-Px levels (P<0.05; Figure 1E and F). These results demonstrate that NBTL administration effectively ameliorated the pathological progression of CIA, highlighting its promising therapeutic potential for clinical applications.

Analysis of the Mechanism of NBTL's Effect on Synovial Tissue in CIA Mice

To elucidate the mechanism underlying NBTL's therapeutic effects on CIA, we specifically investigated its impact on synovial tissue pathology. First of all, Safranin O-fast green staining demonstrated distinct morphological differences among the groups: The synovial tissue in the control group exhibited a smooth surface with uniform staining, while the model group displayed pronounced pathological alterations characterized by an irregular bone surface, extensive tissue damage, faint staining, multiple fissures, and obscured tidemarks. Notably, NBTL treatment significantly ameliorated these pathological features in the NBTL group compared to the model group (Figure 2A). In addition, Western blot analysis demonstrated significant activation of the Fas/FasL pathway in the model group, accompanied by elevated expression of Bax and cl-caspase3 and reduced Bcl-2 levels (P<0.05), indicating enhanced apoptosis in synovial tissue cells. In contrast, the NBTL group exhibited downregulation of Fas/FasL, Bax, and cl-caspase3 compared to the model

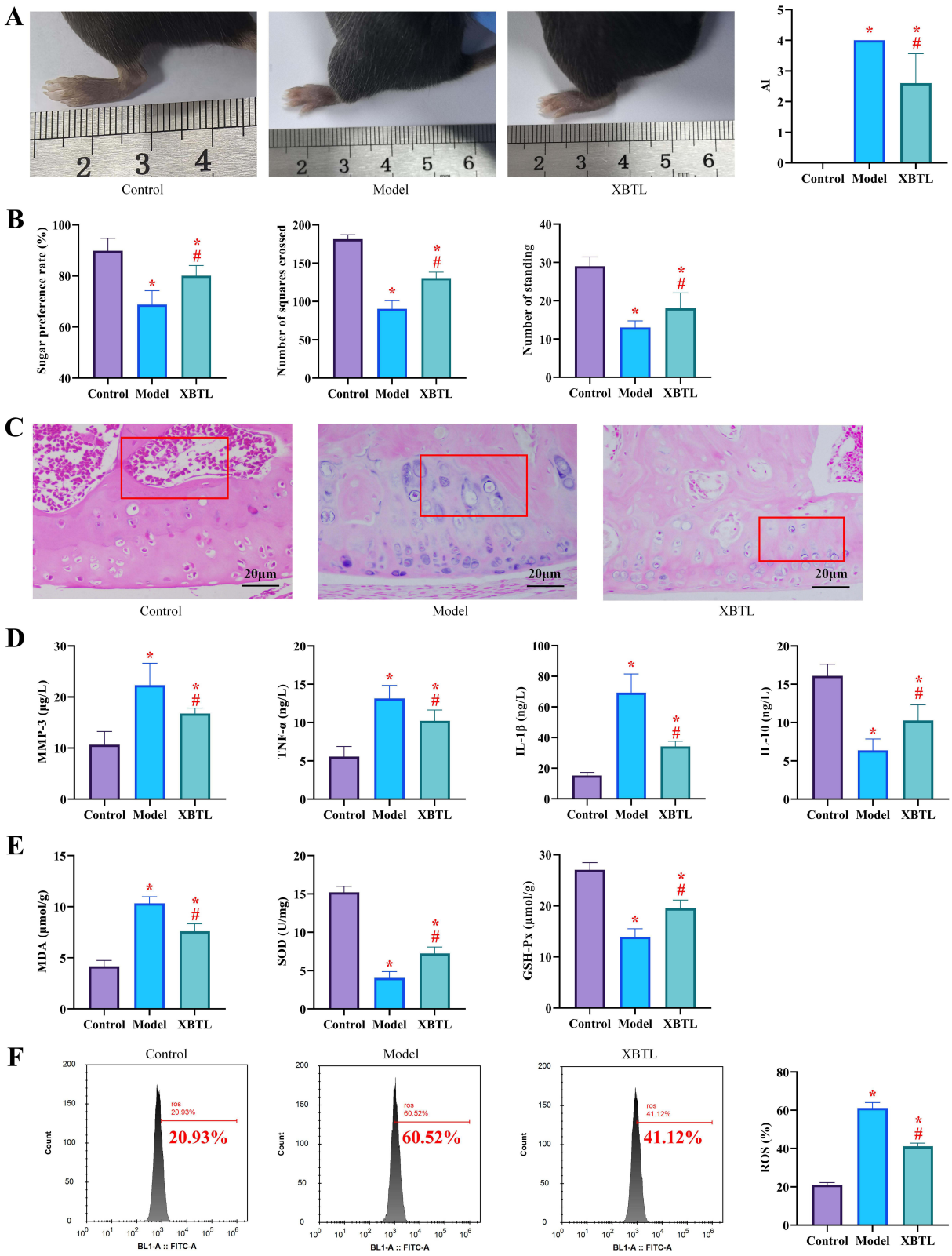

Figure 1 NBTL ameliorates clinical signs and pathologic features in CIA mice (10 rats in each group) (*P<0.05 compared with the control group; #P<0.05 compared with the model group). (**A**) Arthritis Index (AI) scores and swelling of the left hind paw, (**B**) Results of behavioral tests: sucrose preference rate (left) and horizontal activity (middle) and vertical activity (right) of the absent field experiment, (**C**) HE staining of ankle joint tissues showed that the joint structure was normal in the control group, synovial hyperplasia, inflammatory cell infiltration and bone erosion were seen in the model group, and the pathological damage was significantly reduced in the NBTL group, (**D**) Serum inflammatory factor levels (MMP-3, TNF-α, IL-1β and IL-10), (**E**) Indicators of oxidative stress: MDA and ROS levels. (**F**) Antioxidant indicators: SOD and GSH-Px levels.

https://doi.org/10.2147/JIR.S557354

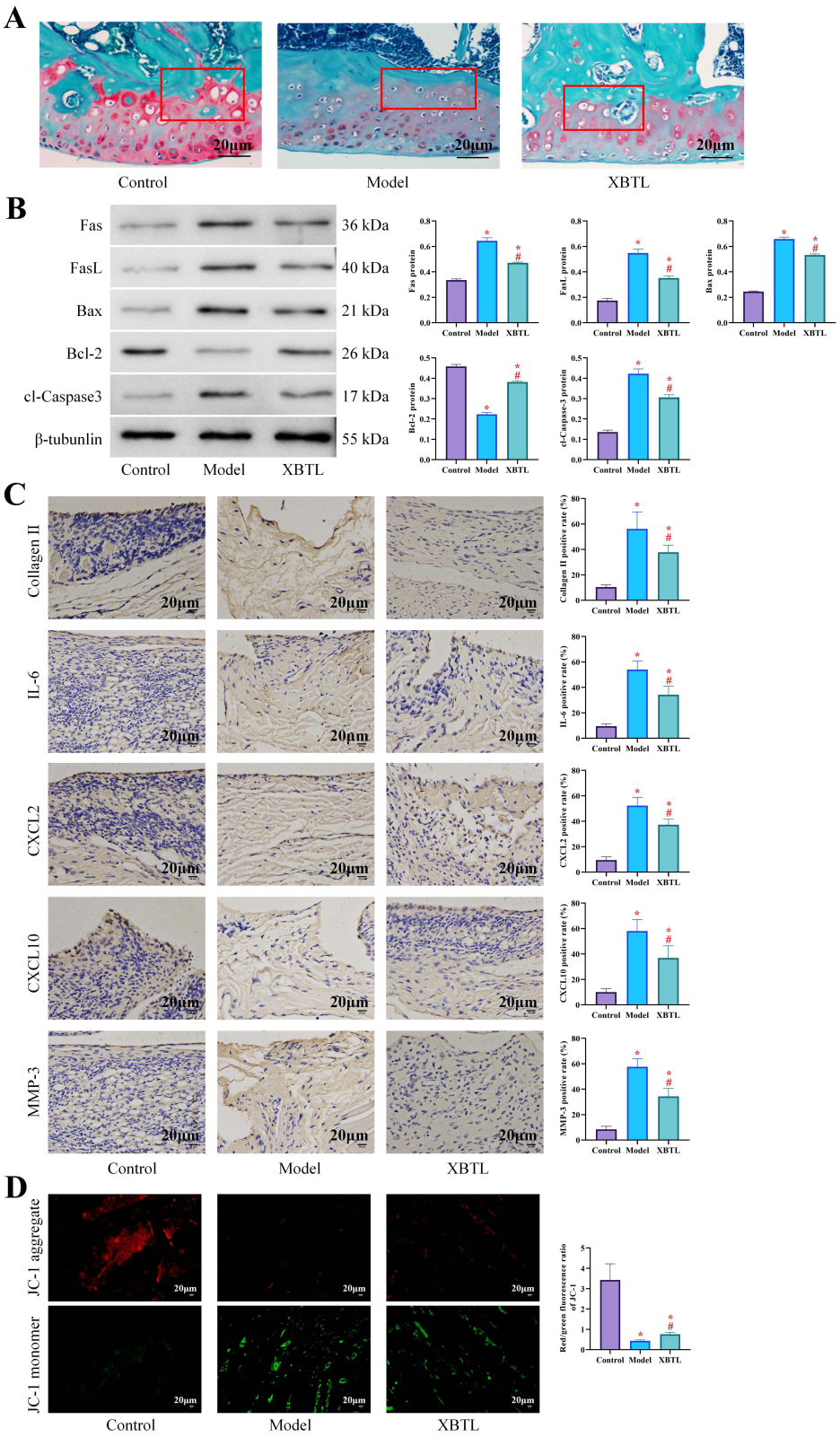

Figure 2 NBTL regulates mitochondrial function and apoptotic pathway in synovial tissue (10 rats in each group) (*P<0.05 compared with the control group; #P<0.05 compared with the model group). (**A**) Safranin O-Fast Green staining of synovial tissue: cartilage surface irregularity in the model group and significant repair in the NBTL group, (**B**) Western blot analysis of apoptosis-related proteins (Fas/FasL, Bax, Bcl-2, cl-caspase3), (**C**) Immunohistochemical staining: Collagen II, IL-6, CXCL2, CXCL10 and MMP-3 positivity in synovial tissue (brown staining), (**D**) JC-1 fluorescence staining: red fluorescence (normal mitochondrial membrane potential), green fluorescence (decreased membrane potential), increased percentage of green fluorescence in the model group, and significant improvement in the NBTL group.

group, while Bcl-2 expression was significantly increased (P<0.05), suggesting suppression of apoptosis (Figure 2B). Immunohistochemical staining further revealed that the model group had significantly higher positive rates of Collagen II, IL-6, CXCL2, CXCL10, and MMP-3 in synovial tissue compared to the control group (P<0.05). Although these markers remained elevated in the NBTL group relative to controls, their expression levels were substantially lower than those in the model group (P<0.05, Figure 2C). According to fluorescence staining analysis, the synovial tissue from the control group exhibited predominantly JC-1 red fluorescence, whereas the model group showed a significant increase in green fluorescence (P<0.05), indicating exacerbated mitochondrial damage. Conversely, the NBTL group displayed a reduced proportion of JC-1 green fluorescence compared to the model group (P<0.05, Figure 2D), suggesting that NBTL ameliorates mitochondrial dysfunction. These findings demonstrate that NBTL mitigates the progression of CIA by attenuating mitochondrial damage and apoptosis in joint synovial tissue.

Impact of NBTL on the Gut Microbiota in CIA Mice

After 16s rDNA sequencing of the fecal samples from the two groups of mice, the end of the dilution curve tended to flatten out, confirming that the testing depth met the requirements, the sequencing quality was good, and the amount of sequencing data reached saturation. Comparing the vertical coordinate, it can be seen that the species abundance of the NBTL group was higher than that of the model group (Figure 3A). α-diversity index analysis showed that the richness, ACE and PD_whole_tree indices of the NBTL group were higher than that of the model group (Figure 3B). In the PCoA, we added 95% confidence ellipses, and it can be seen that the first principal component, PCo1, had a contribution rate of 27.38%, and the contribution of the second principal component, PCo2, had a contribution rate of 27.38%. The contribution of the second principal component PCo2 was 16.51%. The colony structures between the NBTL group and the model group were basically separated, but there still existed overlapping parts, indicating that the composition of the colony structures of the two groups was altered (Figure 3C). Subsequently, Figure 3D demonstrated the differences in gut microbes between the two groups of mice at the Phylum, Classr, Order, Family, Genus and Species levels. In Phylum, the species composition in the fecal samples of the NBTL group and the model group was seen to be basically the same. However, we observed an increase in Firmicutes and a decrease in Verrucomicrobiota in the NBTL group compared to the model group. In Classr, an increase in Clostridia was seen in the NBTL group and a decrease in Verrucomicrobiae decreased. Similarly, in Order, there is also a more significant difference in Verrucomicrobiales between the two groups. In Family, the percentage of Akkermansiaceae decreases in the NBTL group compared to the model group, while Prevotellaceae increases. In Genus, the percentage of Alloprevotella increases significantly in the NBTL group compared to the model group, while Prevotellaceae increased in the NBTL group. Alloprevotella in the NBTL group increased significantly and Prevotellaceae decreased, and this trend was even more pronounced in Species. LEFSe analysis showed that g__Alloprevotella and g__Coriobacteriaceae were the top-ranked groups, indicating that these two species differed significantly between groups (Figure 3E).

Analysis of NBTL-Regulated Target Genes in CIA Mice

Using comparative analysis of fecal samples from the NBTL and model groups, we identified a total of 11 DEGs, of which 5 were up-regulated and 6 were down-regulated (Figure 4A). Functional enrichment analysis showed (Figure 4B) that the main functions of these DEGs were related to biological regulation, cellular anatomical entity, and cellular process. In KEGG analysis, it was seen that DEGs were mainly enriched in Homologous recombination, Parkinson disease, and MAPK signaling pathway. KOG analysis showed that the functional groups of two DEGs were related to Transcription. Among them, ENSMUSG00000018411 (Mapt), which is related to mitochondrial function, attracted our attention (Table 1), so we made it the focus of our subsequent study. In mice, Mapt was similarly elevated in the model group, while it was lower in the NBTL group than in the model group (P<0.05, Figure 4C), as in the above case, which initially suggested that our NBTL might have a role in inhibiting the expression of Mapt.

The Impact of Mapt Modulation on Clinical Manifestations in CIA Mice

To investigate whether NBTL exerts its therapeutic effects on CIA through Mapt-dependent mechanisms, we performed additional experiments following Mapt expression modulation in CIA mice. Initial protein analysis confirmed successful

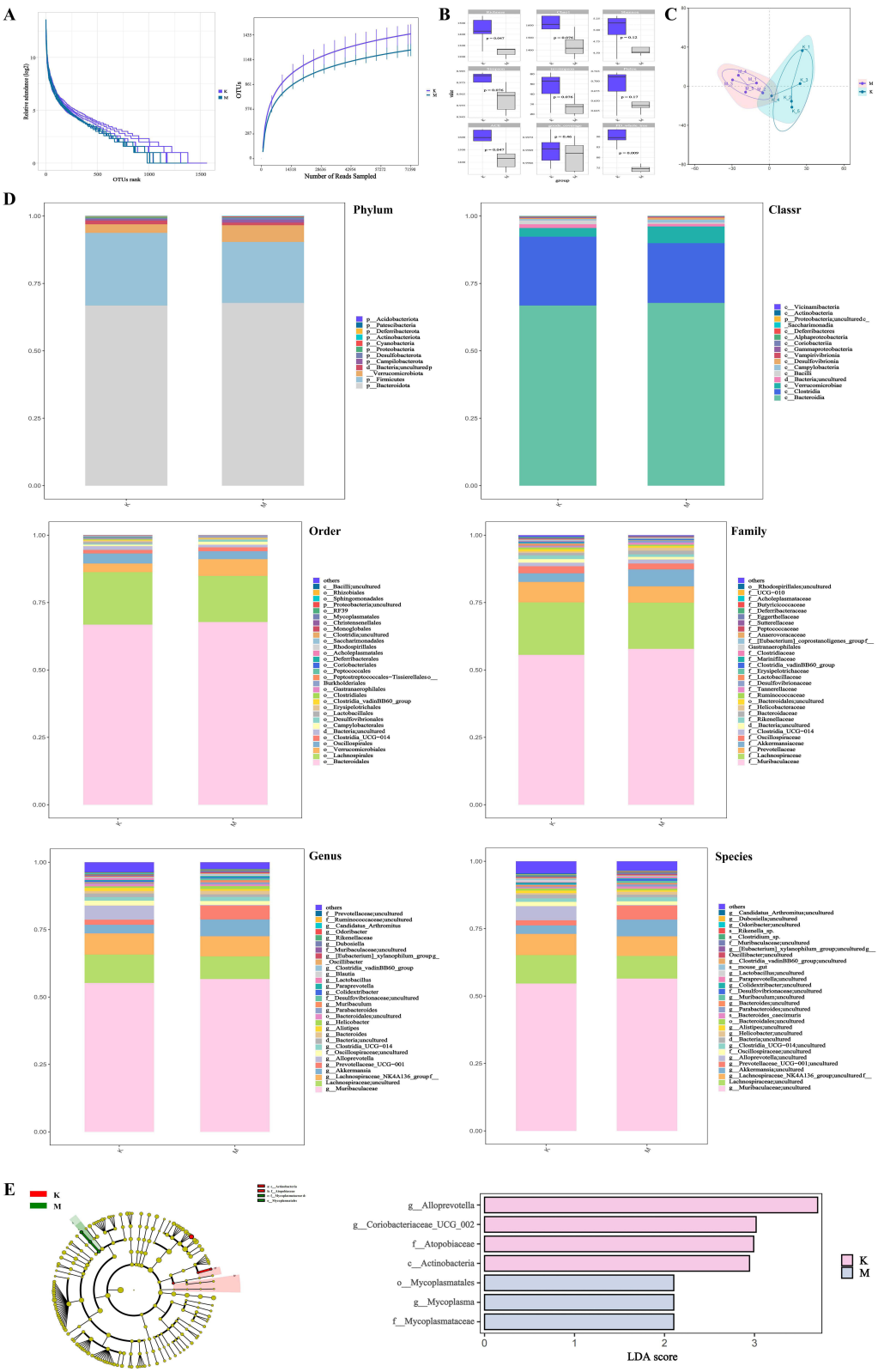

Figure 3 Regulation of intestinal flora by NBTL in CIA mice (10 rats in each group). (**A**) Dilution curve (16S rDNA sequencing data saturation validation), (**B**) α diversity index (Shannon, ACE, PD_whole_tree), (**C**) PCoA analysis (based on Weighted UniFrac distance, 95% confidence ellipse), (**D**) Differences in colony composition at phylum, class, order, family, genus and species level (NBTL group vs model group), (**E**) LEfSe analysis: significantly different bacterial groups (LDA score ≥ 3), eg g__Alloprevotella (up-regulated), g__Coriobacteriaceae (down-regulated).

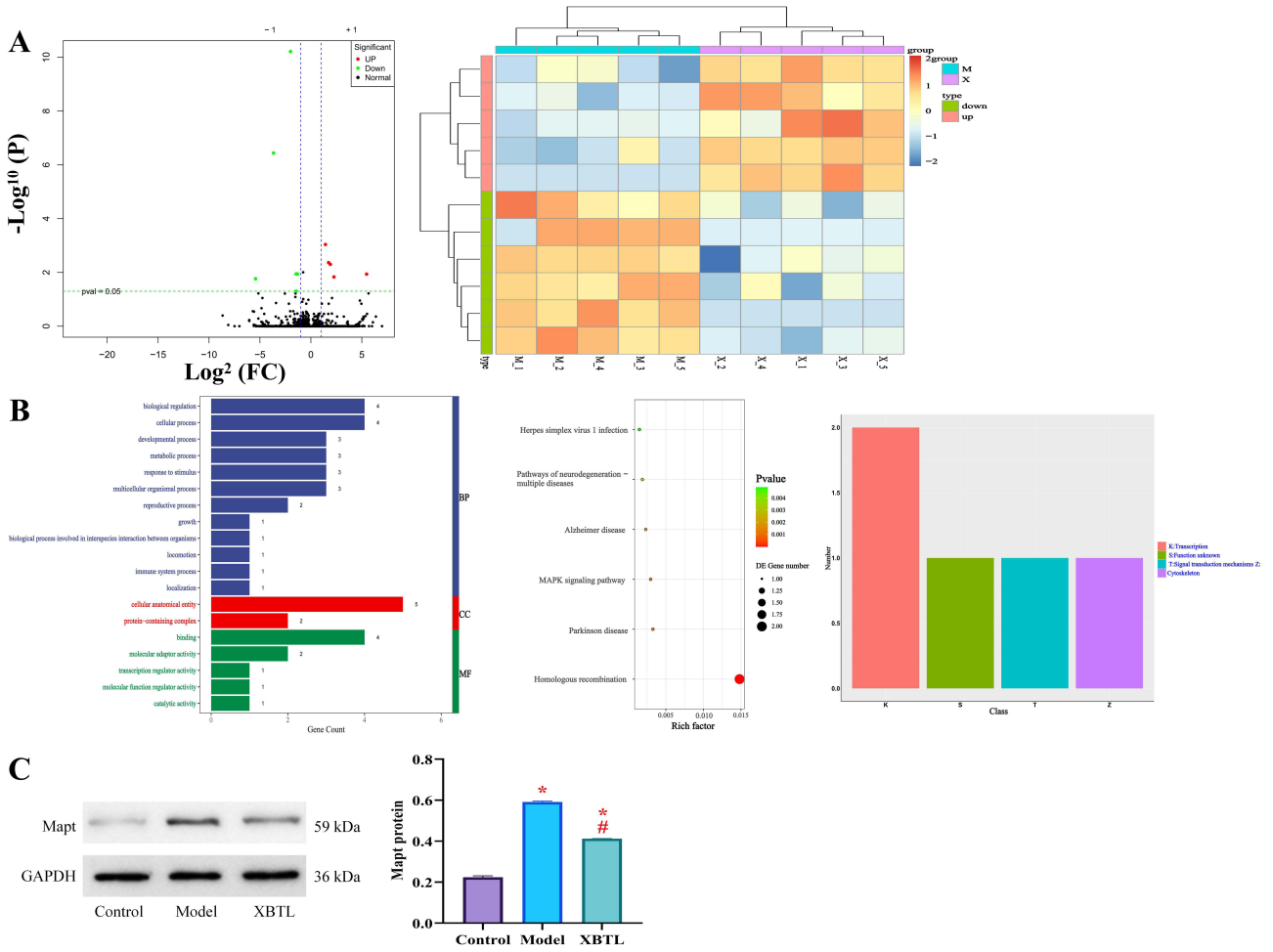

Figure 4 Target gene screening and Mapt validation in NBTL-regulated CIA mice (*P<0.05 compared with the control group; #P<0.05 compared with the model group). (**A**) Volcano plot of differentially expressed genes (DEGs) (red: up-regulated; green: down-regulated), (**B**) Functional enrichment analysis (GO, KEGG, KOG), (**C**) Western blot validation of Mapt protein expression (significantly elevated in the model group and inhibited in the NBTL group) (10 rats in each group).

intervention, with significantly elevated Mapt levels in the upregulation group and reduced expression in the down-regulation group (P<0.05). Notably, the NBTL + upregulation group demonstrated Mapt expression levels comparable to the blank group (P>0.05), suggesting NBTL's ability to normalize Mapt dysregulation (Figure 5A). Subsequent evaluation of joint manifestations revealed that the upregulation group exhibited more severe joint swelling and higher AI scores compared to the blank group, whereas the downregulation group showed significantly milder symptoms (P<0.05). Notably, no statistically significant differences were observed in joint swelling or AI scores between the NBTL + upregulation group and the blank group (P>0.05, Figure 5B). Behavioral analyses yielded congruent results: Mapt overexpression exacerbated disease-associated behavioral impairments (reduced sucrose preference, locomotor activity, and rearing frequency), while Mapt knockdown improved these parameters (P<0.05). NBTL administration with Mapt

Table 1 Effect of Mapt on Mitochondrial Functions

# GO	Name	p_uncorrected
GO:0090258	Negative regulation of mitochondrial fission	0.0016840919677719168
GO:0010917	Negative regulation of mitochondrial membrane potential	0.0028055063739964602
GO:0048312	Intracellular distribution of mitochondria	0.006163453100355139
GO:0090140	Regulation of mitochondrial fission	0.00783888955035947
GO:0051881	Regulation of mitochondrial membrane potential	0.025564245023140163

https://doi.org/10.2147/JIR.S557354

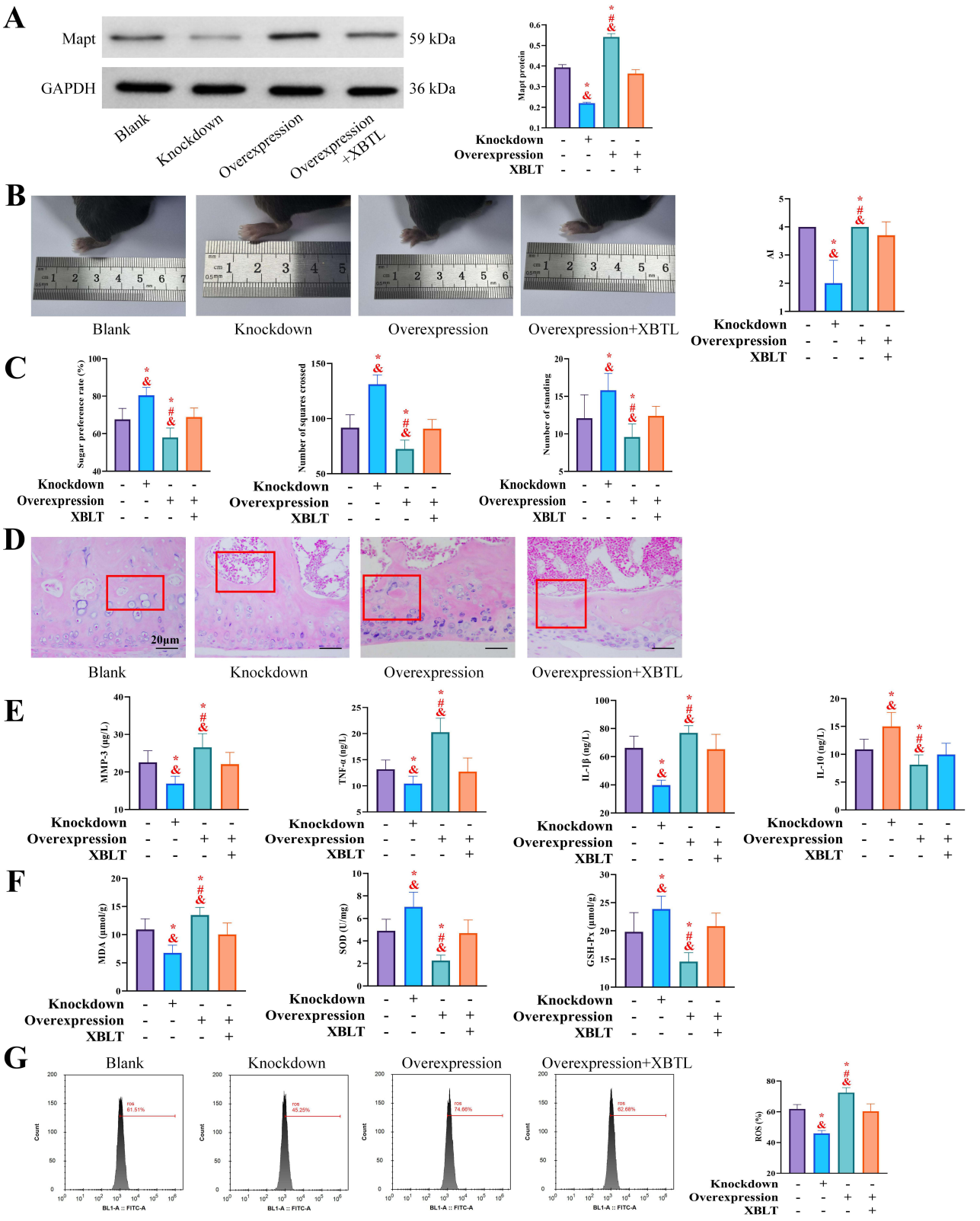

Figure 5 Effect of Mapt expression modulation on the phenotype of CIA mice (10 rats in each group) (*P<0.05 compared with the control group; #P<0.05 compared with the model group; &P<0.05 compared with the overexpression+NBTL group). (**A**) Western blot to verify the efficiency of Mapt intervention (elevated expression in the up-regulated group, suppressed in the down-regulated group and NBTL+ up-regulated group), (**B**) Joint swelling and AI scores (exacerbated in the up-regulated group, restored to normal level in the NBTL+ up-regulated group), (**C**) Behavioral tests (sucrose preference rate, horizontal activity, vertical activity), (**D–G**) Levels of inflammatory factors (MMP-3, TNF-α, IL-1β, IL-10) and oxidative stress indicators (MDA, ROS, SOD, GSH-Px).

upregulation restored normal behavioral patterns indistinguishable from the blank controls (P>0.05, Figure 5C). At the molecular level, Mapt upregulation significantly elevated pro-inflammatory mediators (MMP-3, TNF-α, IL-1β), oxidative stress markers (MDA, ROS), while suppressing anti-inflammatory IL-10 and antioxidant factors (SOD, GSH-Px) (P<0.05). This profile was reversed by Mapt knockdown (P<0.05). Remarkably, no significant differences were observed in the concentrations of inflammatory cytokines or oxidative stress biomarkers between the NBTL + upregulation group and the blank group (P>0.05, Figure 5D–G). These findings demonstrate that Mapt overexpression aggravates CIA pathogenesis, while its suppression ameliorates disease progression. NBTL's therapeutic efficacy appears mediated through the correction of Mapt-mediated pathological mechanisms, effectively reversing the detrimental effects of Mapt upregulation.

Analysis of the Mechanism of Mapt on the Synovial Tissue of CIA Mice

Finally, we analyzed the synovial tissue alterations in the CIA mouse model. Histopathological examination revealed significantly aggravated synovial tissue damage in the Mapt upregulation group compared to the blank group. In contrast, the downregulation group exhibited marked improvement in synovial tissue integrity relative to blank controls. Notably, the NBTL + upregulation group demonstrated synovial characteristics comparable to the blank group (Figure 6A). Furthermore, in the NBTL+ upregulation group, the expression levels of Fas/FasL, Bax, cl-caspase3, and Bcl-2 proteins, along with the positive rates of Collagen II, IL-6, CXCL2, CXCL10, and MMP-3, showed no significant difference compared to the blank group (P>0.05). Notably, the NBTL+ upregulation group exhibited significantly lower levels of Collagen II, IL-6, CXCL2, CXCL10, MMP-3, Fas/FasL, Bax, and cl-caspase3 compared to the upregulation group, while Bcl-2 expression was notably higher (P<0.05, Figure 6B and C). Fluorescence staining demonstrated an increased proportion of JC-1 green fluorescence in the upregulation group (P<0.05), indicative of exacerbated mitochondrial damage. Conversely, the downregulation group exhibited the opposite trend (P<0.05, Figure 6D), suggesting amelioration of mitochondrial dysfunction. Further investigation into the regulatory mechanism of NBTL on Mapt revealed that the Sirtuin 1 (Sirt1)/Peroxisome proliferator-activated receptor γ coactivator 1α (PGC-1α) pathway, which was suppressed in the model group, was reactivated following NBTL intervention (P<0.05). Compared to the model group, the upregulation group showed further inhibition of this pathway, while the downregulation group exhibited enhanced activation (P<0.05). Interestingly, the Sirt1/PGC-1α pathway activity in the NBTL + upregulation group remained unchanged relative to the model group (P>0.05, Figure 6E). These results collectively demonstrate that NBTL modulates Mapt by activating the Sirt1/PGC-1α pathway.

Discussion

As a clinically empirical formula, NBTL demonstrated significant efficacy in mitigating joint damage and attenuating inflammatory responses in CIA mice, primarily through the suppression of Mapt expression. By integrating WGS with molecular biology validation, this study not only elucidated the multidimensional mechanisms underlying NBTL's therapeutic effects but also provided novel molecular pharmacological insights, thereby advancing the modernization of TCM research. Below, we discuss the key mechanisms, potential therapeutic targets, and translational implications of these findings.

Mechanistic Insights into NBTL's Therapeutic Effects on CIA: Modulation of Synovial Tissue Homeostasis

The pathological progression of RA is characterized by two hallmark features: abnormal synovial hyperplasia and inflammatory cell infiltration.[13] Our investigation reveals that NBTL treatment markedly attenuates these pathological manifestations in CIA mice, as evidenced by reduced infiltration of lymphocytes and multinucleated giant cells, along with suppression of pannus formation. These therapeutic effects appear to be mediated through NBTL's comprehensive regulation of chemokine networks and cell migration signaling pathways.[14] At the molecular level, NBTL demonstrates significant inhibitory effects on key inflammatory mediators, including IL-6, CXCL2, CXCL10, and MMP-3. NBTL may disrupt chemokine production through NF-κB nuclear translocation inhibition (as demonstrated by reduced IκBα phosphorylation) and IRF activity modulation, collectively resulting in impaired inflammatory cell recruitment to synovial tissues.[15] Notably,

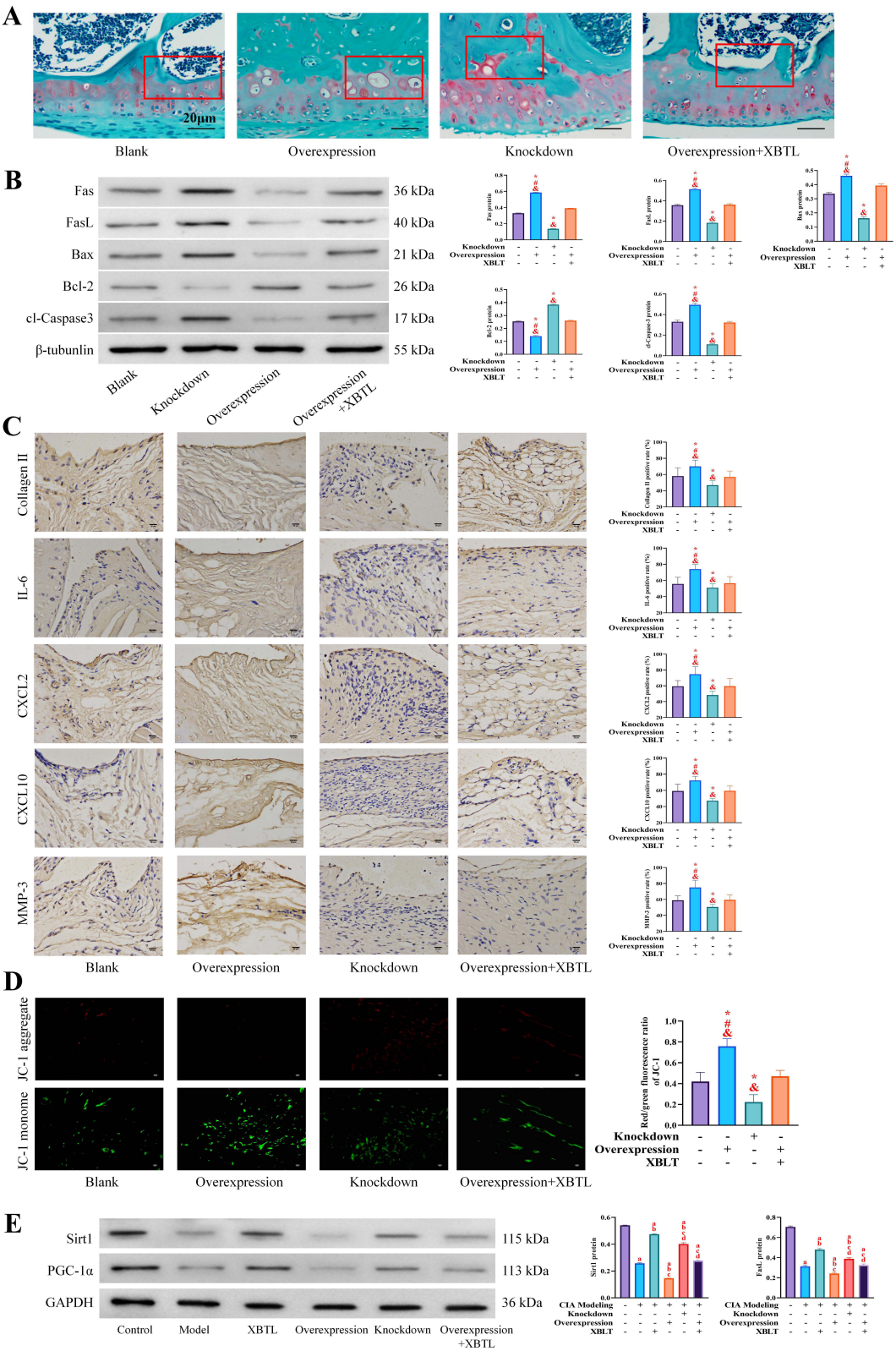

Figure 6 Mapt regulates synovial tissue pathology and Sirt1/PGC-1α pathway (10 rats in each group) (*P<0.05 compared with the control group; #P<0.05 compared with the model group; &P<0.05 compared with the overexpression+NBTL group). (**A**) HE staining of synovial tissue: damage aggravated in the upregulated group and repaired in the NBTL+ upregulated group, (**B**) Western blot analysis of apoptosis-related proteins (Fas/FasL, Bax, Bcl-2, cl-caspase3), (**C**) Immunohistochemical staining: Collagen II, IL-6, CXCL2, CXCL10, MMP-3 positivity, (**D**) JC-1 fluorescence staining (green fluorescence percentage reflects the degree of mitochondrial damage), (**E**) Western blot analysis of Sirt1/PGC-1α pathway activity (inhibited in model group, activated after NBTL intervention).

NBTL also modulates synovial cell apoptosis by downregulating Bax and cl-caspase3 while upregulating the Bcl-2, which may indirectly reshape the inflammatory microenvironment. Fluorescence staining revealed that NBTL markedly decreased the proportion of JC-1 green fluorescence (an indicator of mitochondrial membrane potential collapse) in synovial cells,[16] suggesting its role in restoring mitochondrial integrity and limiting the release of damage-associated molecular patterns (DAMPs), thus disrupting the vicious cycle of inflammation. Furthermore, Western blot analysis demonstrated that NBTL activates the Sirt1/PGC-1α pathway, enhancing mitochondrial biogenesis and antioxidant defenses to mitigate oxidative stress. Collectively, these findings suggest that NBTL restores synovial tissue homeostasis through the cascade of "inhibiting mitochondrial damage → modulating apoptosis → suppressing inflammation", offering a promising multi-target therapeutic strategy for RA treatment.

Regulatory Effects of NBTL on Gut Microbiota Dysbiosis

Gut microbiota dysbiosis has been well-established as a key contributor to systemic inflammation and autoimmune responses in RA patients.[17] A notable example is the disrupted Bacteroidetes-to-Firmicutes ratio, which enhances intestinal permeability and facilitates lipopolysaccharide (LPS) translocation into circulation. This process activates the TLR4/NF-κB pathway, ultimately exacerbating joint inflammation.[18] The study revealed a significant modulation of intestinal flora in CIA mice by NBTL intervention through 16s rDNA sequencing. Sequencing data quality and in-depth validation (saturation of dilution curves) indicated high reliability of the results. Elevated alpha diversity indices (eg, ACE, PD_whole_tree) suggested that NBTL may reshape the intestinal micro-ecological homeostasis by increasing the species richness of the intestinal flora and phylogenetic diversity. This result is consistent with previous studies that the restoration of intestinal flora diversity is closely associated with the remission of autoimmune diseases.[19] PCoA analysis showed that the two groups were partially separated in terms of flora structure (27.38% PCo1 contribution), but there was a region of overlap, implying that although NBTL improved the composition of the flora, it was still potentially affected by individual differences or other environmental factors. Further taxonomic analyses showed that the abundance of Firmicutes phylum increased and Verrucomicrobiota phylum decreased after NBTL intervention, in which the elevated Firmicutes/Bacteroidetes (F/B) ratio may inhibit pro-inflammatory responses by regulating the production of short-chain fatty acid (SCFAs).[20] At the genus level, significant enrichment of Alloprevotella (with suppression of Verrucomicrobiales) may promote intestinal barrier integrity through enhanced butyrate synthesis,[21] and differences in LEfSe analysis of g__Alloprevotella and g__Coriobacteriaceae suggests that it is either the key target flora for NBTL regulation of intestinal inflammation. These findings provide a potential mechanism for NBTL to alleviate CIA through the "colony-immunity" axis. NBTL likely facilitates the "gut-joint axis" communication via two key mechanisms: (1) Enhancing intestinal barrier function to reduce LPS translocation, thereby attenuating excessive TLR4/MyD88 signaling activation; and (2) Modulating microbial metabolites (eg, tryptophan derivatives) to activate the aryl hydrocarbon receptor (AhR), which promotes regulatory T cell (Treg) differentiation while suppressing Th17-driven joint inflammation. While Guan et al proposed NBTL's gut-joint axis via microbiota modulation,[7] our work uncovers a parallel pathway: gut microbiota remodeling → epithelial barrier repair → reduced LPS translocation → dampened MAPT/NF-κB signaling. This dual-action mechanism explains NBTL's superior efficacy compared to single-target therapies.

Molecular Mechanism of NBTL in Regulating Mapt: Multi-Target Synergistic Repair of the Mitochondrial-Inflammatory Axis

Target gene analysis revealed that NBTL intervention affects CIA process by regulating 11 differentially expressed genes (DEGs), among which the aberrant expression of the mitochondria-related gene Mapt (ENSMUSG00000018411) is of particular interest. Mapt, the dysfunction of which is usually associated with abnormal mitochondrial dynamics in neurodegenerative diseases,[22] and the present study suggests for the first time that it may be involved in the intestinal inflammatory process of CIA by regulating mitochondrial ROS generation.[6] Functional enrichment analysis showed that DEGs were mainly involved in "cellular processes" and "biological regulation", and KEGG pathway was enriched in MAPK signaling pathway and Parkinson's disease-related pathway, suggesting that NBTL may be involved in CIA by inhibiting MAPK-mediated pro-inflammatory signals. This mechanism is consistent with the results reported by Chen et al that natural compounds alleviate rheumatoid arthritis through the MAPK/NF-κB pathway.[23] In addition, the predominance

of the "transcription-related" functional group in the KOG classification, combined with the partial colony-gene expression correlation in PCoA, suggests that gut flora remodeling may affect immune homeostasis by regulating host gene transcription through metabolites (eg, SCFAs). However, the direct causal relationship between flora changes and specific gene expression has not yet been clarified in this study, and the synergistic "multi-target-multi-pathway" mechanism of NBTL needs to be further verified in the future by combining metabolomics and gene knockdown modeling. WGS analysis identified Mapt as a core target of NBTL, demonstrating that NBTL ameliorates mitochondrial dysfunction by down-regulating Mapt expression. We hypothesize that NBTL modulates Mapt indirectly through the following mechanisms: (1) Suppression of the NF-κB signaling pathway, thereby attenuating the transcriptional activation of Mapt by pro-inflammatory cytokines; and (2) Enhancement of antioxidant enzyme activity, which mitigates ROS-mediated mtDNA damage and subsequently reduces compensatory Mapt upregulation. This multi-target regulatory network underscores the unique advantage of TCM compounds in achieving "holistic regulation", offering a theoretical foundation for developing novel RA therapeutics with dual anti-inflammatory and mitochondrial-protective effects.

The Impact Mechanism of Mapt on CIA: Mitochondrial Genome Instability Fuels a Vicious Cycle of Synovial Inflammation

Dysregulated expression of Mapt (a critical regulator of mtDNA replication) is closely linked to the molecular pathogenesis of joint damage in RA. Research has demonstrated that Mapt overexpression compromises mtDNA stability, initiating a detrimental cascade of mitochondrial stress–inflammatory amplification–cell death in synovial tissue.[24] This study provides the first evidence that Mapt overexpression aggravates joint swelling, inflammatory cytokine release, and mitochondrial dysfunction in CIA mice, whereas Mapt silencing markedly attenuates these pathological features. Mechanistically, Mapt overexpression may induce mtDNA replication stress, leading to mtDNA deletions or mutations and driving synovial tissue damage through the following pathways: (1) Abnormal mtDNA release activates the cGAS-STING pathway, stimulating type I interferon production and amplifying synovial inflammation.[25] (2) Mitochondrial respiratory chain dysfunction generates excessive ROS, further activating the NLRP3 inflammasome and triggering chondrocyte pyroptosis. (3) Energy metabolism disruption (eg, OXPHOS suppression) shifts synovial fibroblasts (FLS) toward glycolysis-dependent energy production, promoting a pro-inflammatory phenotype.[26] Notably, Mapt overexpression also suppresses the Sirt1/PGC-1α pathway. Sirt1, an NAD+-dependent deacetylase, mitigates inflammatory cytokine release by inhibiting NF-κB transcriptional activity.[27] Thus, Mapt likely orchestrates synovial tissue pathology through a tripartite mechanism encompassing metabolic dysregulation, epigenetic modulation, and inflammatory exacerbation.

Clinical Recommendations and Study Limitations

This study is the first to identify Mapt as a novel therapeutic target for RA and demonstrates that NBTL ameliorates joint damage by suppressing Mapt expression, offering a promising candidate for the development of low-toxicity, long-acting RA therapies. Given its potential modulation of gut microbiota, NBTL may represent a pioneering drug for a multidimensional "immune-metabolic-microbial" therapeutic approach. However, these findings are currently limited to a CIA mouse model, necessitating further validation of Mapt expression patterns in human synovial tissues and clinical samples. The 21-day intervention period only captured the acute phase of CIA progression, limiting insights into long-term NBTL effects. Moreover, the mechanistic link between gut microbiota and Mapt remains unclear, and the specific bioactive components of NBTL, along with their direct molecular targets, require further investigation. For future research, multi-center clinical trials should be initiated to assess the efficacy and safety of NBTL in RA patients. Advanced techniques such as single-cell sequencing and spatial transcriptomics could elucidate the dynamic expression profile of Mapt across synovial cell subpopulations. Additionally, organoid models or gene-editing approaches may help establish the causal relationship between Mapt and the Sirt1/PGC-1α pathway. In recent studies, artificial peroxisomes (AP) have also been considered as a new direction for the treatment of CIA.[28] Therefore, in the follow-up study, we need to compare the differences in the effects of NBTL and AP, so as to provide a more reliable reference for the treatment of CIA.

Conclusion

This study demonstrates that NBTL attenuates joint damage in collagen-induced arthritis mice by suppressing MAPT expression, restoring mitochondrial function, and modulating synovial inflammation. These findings provide preclinical evidence supporting further investigation of NBTL as a novel therapeutic agent for rheumatoid arthritis.

Data Sharing Statement

The data that support the findings of this study are available from the corresponding author upon reasonable request.

Ethical Approval

All the experimental procedures involving animals were conducted in accordance with ARRIVE guidelines and approved by the Animal Ethics Committee of The Affiliated Hospital of Nanjing University of Chinese Medicine (Approval number:2025DW-035-01).

Author Contributions

All authors made a significant contribution to the work reported, whether that is in the conception, study design, execution, acquisition of data, analysis and interpretation, or in all these areas; took part in drafting, revising or critically reviewing the article; gave final approval of the version to be published; have agreed on the journal to which the article has been submitted; and agree to be accountable for all aspects of the work.

Funding

This study was supported by the General Project of the 2024 Provincial Traditional Chinese Medicine Science and Technology Development Plan (No. MS2024017).

Disclosure

The authors report no conflicts of interest in this work.

References

1. Di Matteo A, Bathon JM, Emery P. Rheumatoid arthritis. *Lancet*. 2023;402(10416):2019–2033. doi:10.1016/S0140-6736(23)01525-8
2. Tang Y, Wu Z, Guo R, et al. Ultrasound-augmented anti-inflammatory exosomes for targeted therapy in rheumatoid arthritis. *J Mater Chem B*. 2022;10(38):7862–7874. doi:10.1039/D2TB01219G
3. Diaz-Gonzalez F, Hernandez-Hernandez MV. Rheumatoid arthritis. *Med Clin*. 2023;161(12):533–542. doi:10.1016/j.medcli.2023.07.014
4. Kubo S, Nakayamada S, Tanaka Y. JAK inhibitors for rheumatoid arthritis. *Expert Opin Investig Drugs*. 2023;32(4):333–344. PMID: 37014106. doi:10.1080/13543784.2023.2199919
5. Jang S, Kwon EJ, Lee JJ. Rheumatoid Arthritis: pathogenic Roles of Diverse Immune Cells. *Int J Mol Sci*. 2022;23(2):905. doi:10.3390/ijms23020905
6. Korn L, Speicher AM, Schroeter CB, et al. MAPT genotype-dependent mitochondrial aberration and ROS production trigger dysfunction and death in cortical neurons of patients with hereditary FTLD. *Redox Biol*. 2023;59:102597. doi:10.1016/j.redox.2022.102597
7. Jia N, Ganesan D, Guan H, et al. Mitochondrial bioenergetics stimulates autophagy for pathological MAPT/Tau clearance in tauopathy neurons. *Autophagy*. 2025;21(1):54–79. doi:10.1080/15548627.2024.2392408
8. Guan Y, Zhao X, Lu Y, Zhang Y, Lu Y, Wang Y. New bitongling regulates gut microbiota to predict angiogenesis in rheumatoid arthritis via the gut-joint axis: a deep neural network approach. *Front Microbiol*. 2025;16:1528865. doi:10.3389/fmicb.2025.1528865
9. Li H, Fu S, Shen P, Zhang X, Yang Y, Guo J. Mitochondrial pathways in rheumatoid arthritis: therapeutic roles of traditional Chinese medicine and natural products. *Phytomedicine*. 2025;146:157106. doi:10.1016/j.phymed.2025.157106
10. Miyoshi M, Liu S. Collagen-induced arthritis models. *Methods Mol Biol*. 2024;2766:3–7.
11. Zhao X, Li M, Lu Y, et al. Sirt1 inhibits macrophage polarization and inflammation in gouty arthritis by inhibiting the MAPK/NF-kappaB/AP-1 pathway and activating the Nrf2/HO-1 pathway. *Inflamm Res*. 2024;73(7):1173–1184. doi:10.1007/s00011-024-01890-9
12. Ba X, Wang H, Huang Y, et al. Simiao pill attenuates collagen-induced arthritis and bleomycin-induced pulmonary fibrosis in mice by suppressing the JAK2/STAT3 and TGF-beta/Smad2/3 signalling pathway. *J Ethnopharmacol*. 2023;309:116274. doi:10.1016/j.jep.2023.116274
13. Van Mechelen M, Martens T, Vanden Berghe P, Lories R, Gulino GR. Impact of barrier tissue inflammation and physical activity on joint homeostasis in mice. *Rheumatology*. 2022;61(4):1690–1698. doi:10.1093/rheumatology/keab517
14. Wang L, Wu X, Wan Q, Yang Y, Gao C. Phloridzin reduces synovial hyperplasia and inflammation in rheumatoid arthritis rat by modulating mTOR pathway. *Int Immunopharmacol*. 2024;133:111727. doi:10.1016/j.intimp.2024.111727
15. Mussbacher M, Derler M, Basilio J, Schmid JA. NF-kappaB in monocytes and macrophages - an inflammatory master regulator in multitalented immune cells. *Front Immunol*. 2023;14:1134661. doi:10.3389/fimmu.2023.1134661

16. Zhu S, Li X, Dang B, Wu F, Wang C, Lin C. Lycium Barbarum polysaccharide protects HaCaT cells from PM2.5-induced apoptosis via inhibiting oxidative stress, ER stress and autophagy. *Redox Rep*. 2022;27(1):32–44. doi:10.1080/13510002.2022.2036507
17. Attur M, Scher JU, Abramson SB, Attur M. Role of intestinal dysbiosis and nutrition in rheumatoid arthritis. *Cells*. 2022;11(15):2436. doi:10.3390/cells11152436
18. Nguyen NT, Sun WH, Chen TH, Tsai PC, Chen CC, Huang SL. Gut mucosal microbiome is perturbed in rheumatoid arthritis mice and partly restored after TDAG8 deficiency or suppression by salicylanilide derivative. *Int J Mol Sci*. 2022;23(7). doi:10.3390/ijms23073527
19. Wastyk HC, Fragiadakis GK, Perelman D, et al. Gut-microbiota-targeted diets modulate human immune status. *Cell*. 2021;184(16):4137–4153e4114. doi:10.1016/j.cell.2021.06.019
20. Quaglio AEV, Grillo TG, De Oliveira ECS, Di Stasi LC, Sassaki LY. Gut microbiota, inflammatory bowel disease and colorectal cancer. *World J Gastroenterol*. 2022;28(30):4053–4060. doi:10.3748/wjg.v28.i30.4053
21. Chen D, Xiong J, Feng H, Liu Y, Xu J, Xu H. The influence of mosapride on gut microbiota of carbon tetrachloride-induced cirrhosis rats based on 16S rRNA gene sequencing. *Adv Clin Exp Med*. 2022;31(6):623–633. doi:10.17219/acem/146320
22. Zhang XX, Wei M, Wang HR, Hu YZ, Sun HM, Jia JJ. Mitochondrial dysfunction gene expression, DNA methylation, and inflammatory cytokines interaction activate Alzheimer's disease: a multi-omics Mendelian randomization study. *J Transl Med*. 2024;22(1):893. doi:10.1186/s12967-024-05680-z
23. Chen H, Zheng M, Zhang W, Long Y, Xu Y, Yuan M. Research status of mouse models for Non-Small-Cell Lung Cancer (NSCLC) and Antitumor Therapy of Traditional Chinese Medicine (TCM) in mouse models. *Evid Based Complement Alternat Med*. 2022;2022:6404853. doi:10.1155/2022/6404853
24. Andres-Benito P, Flores A, Busquet-Areny S, et al. Deregulated transcription and proteostasis in adult mapt knockout mouse. *Int J Mol Sci*. 2023;24(7):6559. doi:10.3390/ijms24076559
25. Jimenez-Loygorri JI, Villarejo-Zori B, Viedma-Poyatos A, et al. Mitophagy curtails cytosolic mtDNA-dependent activation of cGAS/STING inflammation during aging. *Nat Commun*. 2024;15(1):830. doi:10.1038/s41467-024-45044-1
26. Zheng Y, Wei K, Jiang P, et al. Macrophage polarization in rheumatoid arthritis: signaling pathways, metabolic reprogramming, and crosstalk with synovial fibroblasts. *Front Immunol*. 2024;15:1394108. doi:10.3389/fimmu.2024.1394108
27. Li HR, Liu Q, Zhu CL, et al. beta-Nicotinamide mononucleotide activates NAD+/SIRT1 pathway and attenuates inflammatory and oxidative responses in the hippocampus regions of septic mice. *Redox Biol*. 2023;63:102745. doi:10.1016/j.redox.2023.102745
28. Wang L, Zhang L, Chen F, et al. Polymerized network-based artificial peroxisome reprogramming macrophages for photoacoustic imaging-guided treatment of rheumatoid arthritis. *ACS Appl Mater Interfaces*. 2024;16(20):25856–25868. doi:10.1021/acsami.4c04000